Light Scattering Measurements of Subcellular Structure Provide Noninvasive Early Detection of Chemotherapy-Induced Apoptosis

Kevin J. Chalut,[1] Julie Hanson Ostrander,[2] Michael G. Giacomelli,[1] and Adam Wax[1]

[1]Department of Biomedical Engineering, Fitzpatrick Institute for Photonics, Duke University and [2]Department of Medicine, Division of Medical Oncology, Duke University Medical Center, Durham, North Carolina

Abstract

We present a light scattering study using angle-resolved low coherence interferometry (a/LCI) to assess nuclear morphology and subcellular structure within MCF-7 cells at several time points after treatment with chemotherapeutic agents. Although the nuclear diameter and eccentricity are not observed to change, the light scattering signal reveals a change in the organization of subcellular structures that we interpret using fractal dimension (FD). The FD of subcellular structures in cells treated with paclitaxel and doxorubicin is observed to increase significantly compared with that of control cells as early as 1.5 and 3 hours after application, respectively. The FD is then found to decrease slightly at 6 hours postapplication for both agents only to increase again from 12 to 24 hours posttreatment when the observations ceased. The changes in structure appear over two time scales, suggesting that multiple mechanisms are evident in these early apoptotic stages. Indeed, quantitative image analysis of fluorescence micrographs of cells undergoing apoptosis verifies that the FD of 4′,6-diamidino-2-phenylindole–stained nuclear structures does not change significantly in cells until 12 hours after treatment, whereas that of MitoTracker stained mitochondria is seen to modulate as early as 3 hours after treatment. In contrast, cells receiving an increased dose of paclitaxel that induced G_2-M arrest, but not apoptosis, only exhibited the early change in subcellular structure but did not show the later change associated with changes in nuclear substructure. These results suggest that a/LCI may have utility in detecting early apoptotic events for both clinical and basic science applications. [Cancer Res 2009;69(3):1199–204]

Introduction

Dysregulation of programmed cell death, apoptosis, has important implications in normal development and disease. A key step in cancer initiation and progression is escape from normal apoptotic controls that lead to the elimination of cancer cells (1). In addition, defective apoptotic signaling results in cancer cells that may be resistant to, or become resistant to, chemotherapeutic treatments. Extensive research has been done and is currently under way to understand apoptotic signaling pathways and how these pathways are perturbed in cancer and other diseases (2). Additional efforts are being put forth to develop technologies to detect apoptosis *in vivo* (3). Noninvasive *in vivo* detection of apoptosis has great potential to enhance our ability to monitor patients undergoing cancer therapy and could provide rapid feedback on whether a patient is responding to current conventional therapies or newly developed drugs. Currently, many noninvasive imaging techniques require radioactive labels and contrast agents (3). We aim to develop an optical technology that uses endogenous contrast to detect early structural changes characteristic of apoptosis.

Two distinct modes of apoptosis have been described, extrinsic and intrinsic. Extrinsic activation of apoptosis is dependent on activation of death receptors (i.e., TNFR family), whereas intrinsic apoptosis activation results from disruption of intracellular homeostasis (DNA damage, cellular stress). Taxanes and anthracyclines, such as paclitaxel and doxorubicin, respectively, are used to treat a variety of types of cancer and lead to the activation of intrinsic apoptotic pathways. Paclitaxel enhances microtubule stability, resulting in G_2-M arrest and apoptosis. Doxorubicin is a topoisomerase II inhibitor and inhibits DNA and RNA synthesis. Although these two chemotherapy agents have different mechanisms of action, both have been shown to induce apoptosis in MCF-7 breast cancer cells (4, 5). We aim to determine if similar changes in subcellular structure after drug treatment can be detected using light scattering methods.

Intrinsic and extrinsic apoptosis both result in a highly ordered apoptotic process that is characterized by specific morphologic and biochemical changes. Morphologic changes include chromatin condensation, cell shrinkage, and membrane blebbing (2). Common biochemical events include translocation of phosphotidylserine to the outer plasma membrane, caspase activation, and DNA fragmentation (2). These common morphologic and biochemical characteristics have directed the study of molecular events associated with apoptosis and resistance to apoptotic stimuli. For example, there are numerous assays available to identify DNA fragmentation, an end result of apoptosis. These include flow cytometry approaches in which DNA from fixed cells is labeled with an exogenous dye, such as propidium iodide, 4′,6-diamidino-2-phenylindole (DAPI), or Hoescht, and then cellular DNA content is examined on a cell by cell basis (6). Additionally, there are assays for caspase activation, which involve incubating live cells or a cellular lysate with a caspase cleavage site conjugated to an exogenous fluorophore (chromophore) that fluoresces (absorbs) once cleaved (7). Assays that differentiate early and late apoptotic events use Annexin V fluorescent conjugates, which bind to the exposed phosphotidylserine, in combination with dyes (i.e., propiduim iodide, 7-AAD) that only enter cells after loss of membrane integrity (6). Although more recent data indicates that additional subcellular structural and functional changes commonly occur during early apoptosis (8–10), techniques that provide early, noninvasive detection of apoptosis have been previously unavailable.

Note: Supplementary data for this article are available at Cancer Research Online (http://cancerres.aacrjournals.org/).

K.J. Chalut and J.H. Ostrander contributed equally to this work.

Requests for reprints: Adam Wax, Department of Biomedical Engineering, Box 90281, Duke University, Durham, NC 27708. Phone: 919-660-5143; Fax: 919-684-4488; E-mail: a.wax@duke.edu.

doi:10.1158/0008-5472.CAN-08-3079

In the present study, we applied angle-resolved low coherence interferometry (a/LCI; refs. 11, 12), a noninvasive light scattering technique that is highly sensitive to changes in subcellular structure, to the study of apoptosis in MCF-7 breast cancer cells. The a/LCI technique provides an alternative to imaging for probing subcellular morphology. With this method, the change in momentum of photons due to interaction with a sample is examined to quantitatively probe its structure (13). The main advantage of a/LCI is that it is a nonperturbative optical modality, i.e., it uses light in the spectral region known as the "therapeutic window" for optical imaging (near IR wavelengths; ref. 14). The optical therapeutic window is especially important for *in vivo* diagnostic techniques because major tissue chromophores, such as water, hemoglobin, and melanin, do not absorb light at these wavelengths. We show that, by using a/LCI to measure the fractal dimension (FD) of structures within MCF-7 cells treated with paclitaxel and doxorubicin, we can sensitively distinguish between control cells and cells undergoing apoptosis within three hours of treatment.

The a/LCI method has been developed to detect neoplasia in animal models by measuring changes in nuclear morphology (15, 16) and, more recently, has been applied to assess nuclear deformation in studies of cellular response to environmental stimuli (17). A/LCI and other light scattering techniques have shown the ability to assess FD in biological samples (13, 15, 18, 19). Moreover, light scattering techniques, including a/LCI, have been used to assess apoptosis *in vivo* (15) and in cell studies (20–23). The present study extends this previous work by sensitively detecting early changes in response to apoptosis-inducing chemotherapeutic drugs. Additionally, the present study points to FD as an important indicator of structural changes in cells specifically related to apoptosis. Finally, mechanisms for structural changes that affect the FD are quantified and explored to better understand the rubric of FD and its potential for indicating apoptosis.

Materials and Methods

a/LCI. a/LCI, which is outlined in detail in references (11, 12), obtains depth-resolved measurements of the far-field diffraction of a biological sample, which corresponds to a cell monolayer in the present study. Low coherence interferometry permits the rejection of multiply scattered light that can cause noise artifacts in the signal. The signal resulting from an a/LCI measurement is processed to isolate the scattering from individual cell nuclei and all smaller organelles in the ensemble while eliminating contributions from long range correlations within the monolayer (24). The processed nuclear scattering profile is then analyzed using an inverse light scattering analysis (ILSA) algorithm to determine the properties of the nucleus (shape, size, etc.). Traditional ILSA algorithms for analyzing scattering from biological samples have generally used Mie theory, a model of spherical scatterers; however, in the present study, the ILSA algorithm uses a T-matrix light scattering model (25), which predicts scattering from spheroidal scatterers. The T matrix–based ILSA algorithm has been shown to yield accurate measurements of the average equal volume diameter, EVD, and the average aspect ratio, ε, of stretched microspheres in tissue phantoms (26) and cell nuclei in monolayers (27).

The predicted nuclear scattering profile can now be subtracted from the original data, which comprises nuclear scattering plus scattering due to smaller organelles, to isolate the slowly varying background in the scattering signal, which corresponds to smaller organelles (smaller than ~ 2 μm). This residual scattering signal is Fourier transformed to yield the two-point density correlation function of small organelles, which generally exhibits a power law function. Density correlations that obey a power law indicate self-similarity in a distribution (28); in the cellular materials investigated in the present study, the power law form held over one to two orders of magnitude of size scale (13). The exponent of the power law can be physically interpreted as representing a mass fractal in three dimensions, and can be used to deduce the mass FD.

The T-matrix database used for the ILSA algorithm computed scattering from spheroidal particles with EVD ranging from 7.8 to 12.2 μm, ε ranging from 0.56 to 0.9, size distributions of 7% and 10%, background index of refraction from 1.35 to 1.36, and scattering refractive index from 1.42 to 1.43. These ranges of values are based on quantitative image analysis of MCF-7 cell samples and published values for cellular refractive indices (29). A least-squares fitting of the processed scattering data were used in the ILSA algorithm to determine the most probable scattering configuration from the database. For more extensive details concerning a/LCI optics, processing of the a/LCI signal, the ILSA algorithm, and the statistical techniques, please see Supplementary Methods.

Cell culture. MCF-7 breast cancer cells, obtained from the Duke University Cell Culture facility, were maintained in minimal essential medium α (Invitrogen), supplemented with 5% fetal bovine serum, 10 mmol/L HEPES (Invitrogen), 1× nonessential amino acids (Invitrogen), 1× sodium pyruvate (Invitrogen), 1 μg/mL insulin (Invitrogen), 1 μg/mL hydrocortisone (Sigma), and 10 ng/mL epidermal growth factor (Sigma). For a/LCI measurements, MCF-7 cells were plated at 2.5×10^5 cells per well in 2-well chamber slides and incubated over night at 37°C, 5% CO_2. For all treated samples, 5 or 50 nmol/L paclitaxel (sigma), or 5 μmol/L doxorubicin (EMD biosciences) was added to growth medium and then the cellular medium was replaced. The medium for the control (untreated) cells was changed at the beginning of the experiment as well.

Flow cytometry. MCF-7 cells were plated at 2.5×10^5 cells per well in 6-well plates and treated in triplicate with either vehicle control (DMSO), 5 nmol/L, or 50 nmol/L paclitaxel for indicated times. Cell were trypsinized, pelleted by centrifugation, and then fixed with 80% ethanol. Samples were placed at −20°C until the day of analysis. On the day of analysis, cell pellets were washed twice with PBS and then resuspended in 300 μL of fluorescence-activated cell sorting buffer (1.37 mol/L NaCl, 27 mmol/L KCl, 43 mmol/L Na_2HPO_4, 14.7 mmol/L KH_2PO_4, 1 mg/mL RNase A, 0.5 mmol/L EDTA, 0.1% Triton X-100, and 0.2 mg/mL propidium iodide). Samples were analyzed by the Duke University Flow Cytometry facility for DNA content.

Quantitative image analysis. MCF-7 cells were plated at 1×10^5 cells per well in 4-well chamber slides and treated as described above. All treatment groups were fixed in 4% paraformaldehyde and nuclei were stained with DAPI (Sigma Aldrich). Samples were thoroughly washed with PBS and mounted onto glass coverslips with Vectashield (Vector Laboratories) before images were obtained with fluorescence microscopy (Fig. 4*A* and *B*). Each sample was imaged (×40) at 3 to 4 separate regions at T = 3, 6, 12, and 24 h. These images were analyzed using ImageJ NIH image processing software. Reported nuclear diameters are based on size determinations for $n = 70$ cells. To compute box counting FD (box FD), distinct cell nuclei were individually isolated and analyzed for a total of ~ 40 cell nuclei for each posttreatment time point. Each isolated nucleus was converted to a binary image and the box FD was computed using the built-in FD function in ImageJ. Box sizes of 2,3,4,6,8,12,16,32,64 pixels were used. An important distinction exists between the box FD, which is computed from two-dimensional images, and the mass FD, which is computed from the a/LCI data as a three-dimensional mass fractal (13). At all times in the text, FD as computed by quantitative image analysis (QIA) will be called box FD, and FD as computed by a/LCI will be called mass FD.

For MitoTracker experiments, MCF-7 cells were plated at 2.5×10^5 cells per dish in 35-mm glass-bottom dishes (MatTek) and incubated overnight at 37°C, 5% CO_2. The following day, MCF-7 cells were treated with 5 nmol/L paclitaxel for 3, 6, and 12 h. For control samples, the growth medium was changed and cells were incubated in parallel to paclitaxel treated samples. One hour before imaging, 100 nmol/L MitoTracker FM Green was added to all samples. MitoTracker images were acquired using a Leica SP5 confocal microscope (Duke University Light Microscopy Core Facility). MitoTracker FM Green was excited at 488 nm and emission spectra were collected from 510 to 580 nm. Three to 4 images were taken per plate, 2 plates per

treatment group, per time point with a ×40/1.25 Oil objective (Fig. 4*C* and *D*). The box FD was computed as described above on a per cell basis ($n \geq 40$).

Statistical methods. All *P* values were calculated by using a rank sum test in Matlab using the default value of $\alpha = 0.05$.

Results

Paclitaxel induces apoptosis and G_2-M arrest in MCF-7 cells. To determine the optimal concentration of paclitaxel to induce apoptosis in MCF-7 cells, cells were treated with increasing concentrations of paclitaxel (0, 1, 5, 10, 25 and 50 nmol/L) for 24 hours. Cells were fixed and stained with propidium iodide. Flow cytometry cell cycle analysis showed that compared with control cells (6.48% ± 1.23%), 1 and 5 nmol/L concentrations of paclitaxel induced a significant increase in the percentage of cells with a sub-G_1 content of DNA, 18.26% ± 1.27% and 21.03% ± 2.55%, respectively (Fig. 1). Furthermore, higher concentrations of paclitaxel (10, 25, and 50 nmol/L), only induced an increase in cells arrested in G_2-M and not apoptosis (Fig. 1). To determine the optimal time of exposure, MCF-7 cells were either left untreated or treated with 5 nmol/L paclitaxel for 3, 6, 9, and 24 hours and fixed and stained with propidium iodide for cell cycle analysis. As shown in Fig. 2, 5 nmol/L paclitaxel induced a significant increase in cells with sub-G_1 content of DNA within 6 hours, 3.0 ± 0.42 in control cells to 5.07 ± 0.25 in paclitaxel-treated cells. By 24 hours, ~30% of the paclitaxel-treated cells were apoptotic. A similar set of experiments were performed with doxorubicin. We determined that the optimal concentration of doxorubicin to induce apoptosis in MCF-7 cells was 5 μmol/L, and, similar to paclitaxel-treated MCF-7 cells, an increase in apoptotic cells was observed within 6 hours of treatment (data not shown).

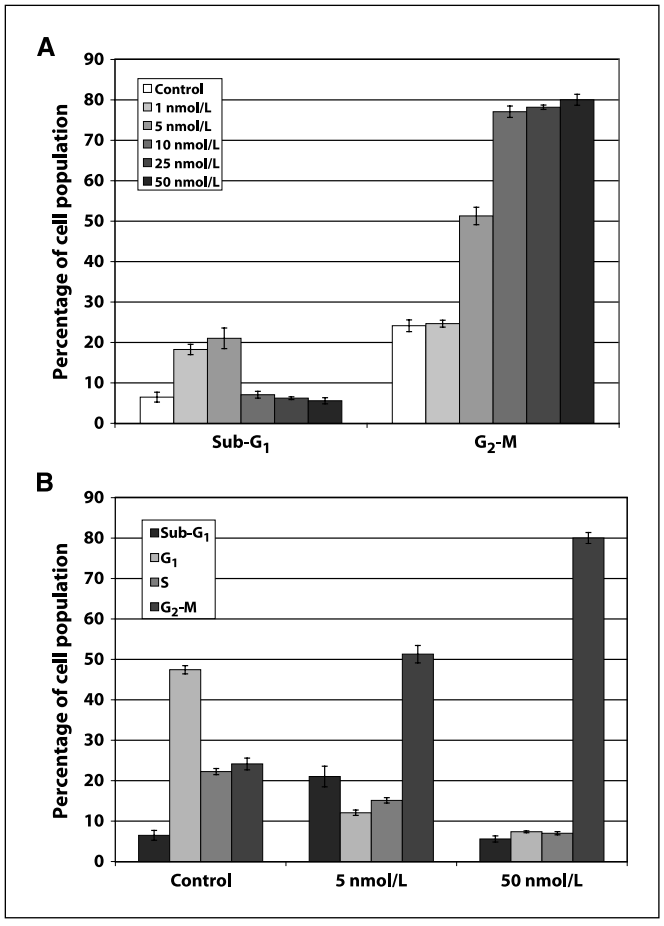

Figure 1. Paclitaxel induces apoptosis and G_2-M arrest in MCF-7 breast cancer cells. *A,* control MCF-7 cells and cells treated for 24 h with 1, 5, 10, 25, and 50 nmol/L paclitaxel were fixed and stained with propidium iodide and then analyzed by flow cytometry for cellular DNA content. Results shown in *A* are only the sub-G_1 and G_2-M (4n) DNA content populations. *B,* complete cell cycle analysis from control MCF-7 cells and cells treated with 5 and 50 nmol/L paclitaxel for 24 h.

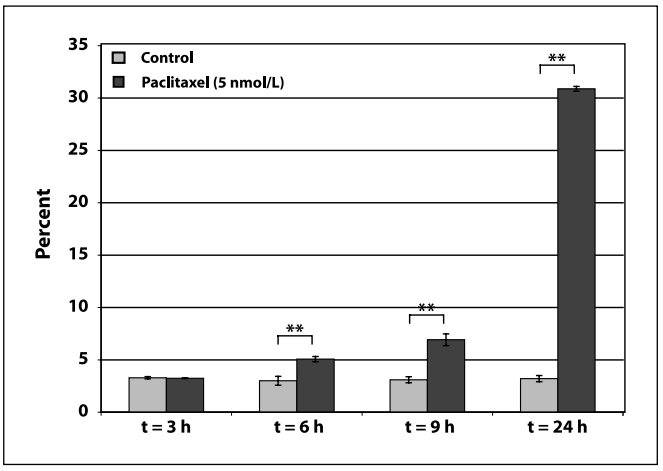

Figure 2. Paclitaxel-treated MCF-7 cells show significant DNA fragmentation within 6 h of treatment. Control and 5 nmol/L paclitaxel-treated MCF-7 cells (3, 6, 9, and 24 h) were stained with propidium iodide and analyzed by flow cytometry for DNA content; data shown is only the percentage of the cellular population with sub-G_1 DNA content. **, high statistical significance ($P < 0.001$).

a/LCI FD. Using T-matrix theory-based ILSA, the size and shape of the MCF-7 cell nuclei (EVD) was found to agree with the results of QIA of DAPI-stained samples to a high degree of accuracy (Supplementary Fig. S3). We found no significant changes in nucleus EVD or aspect ratio for treated or control cells throughout the observation window, using either the a/LCI technique or QIA.

No discernible pattern was observed for the mass FD of the paclitaxel-treated MCF-7 cells when using Mie theory–based ILSA (Supplementary Fig. S2). Therefore, the T matrix–based ILSA algorithm described above was instead used to determine the mass FD of control MCF-7 cells and cells treated with 5 nmol/L paclitaxel. These results show an increase in mass FD from D = 1.63 ± 0.44 (in the form of mean ± SD) to D = 2.13 ± 0.13 from t = 0 to 3 hours but then regressed slightly at t = 6 hours to 1.95 ± 0.17. The mass FD increased to 2.00 ± 0.24 and 2.02 ± 0.14 at 12 and 24 hours, respectively. The mass FD of control cells ranges from 1.50 to 1.70 with SD ranging from 0.20 to 0.40. The mass FD of treated cells at t = 3, 12, and 24 hours shows statistically significant differences from both control cells and treated cells at t = 0 hours. The difference between the mass FD of treated cells at t = 6 hours and control cells at the same time point are also statistically significant, but at this time point, there is not a statistical significance between treated cells at t = 0. All results from treated and control groups are shown in Fig. 3*A*, which also indicates where results are statistically significant.

To determine if the paclitaxel-induced changes in FD are specific to taxane-based chemotherapy treatments, MCF-7 cells were treated with doxorubicin, an anthracyline that inhibits topoisomerase II and inhibits DNA and RNA synthesis. MCF-7 cells

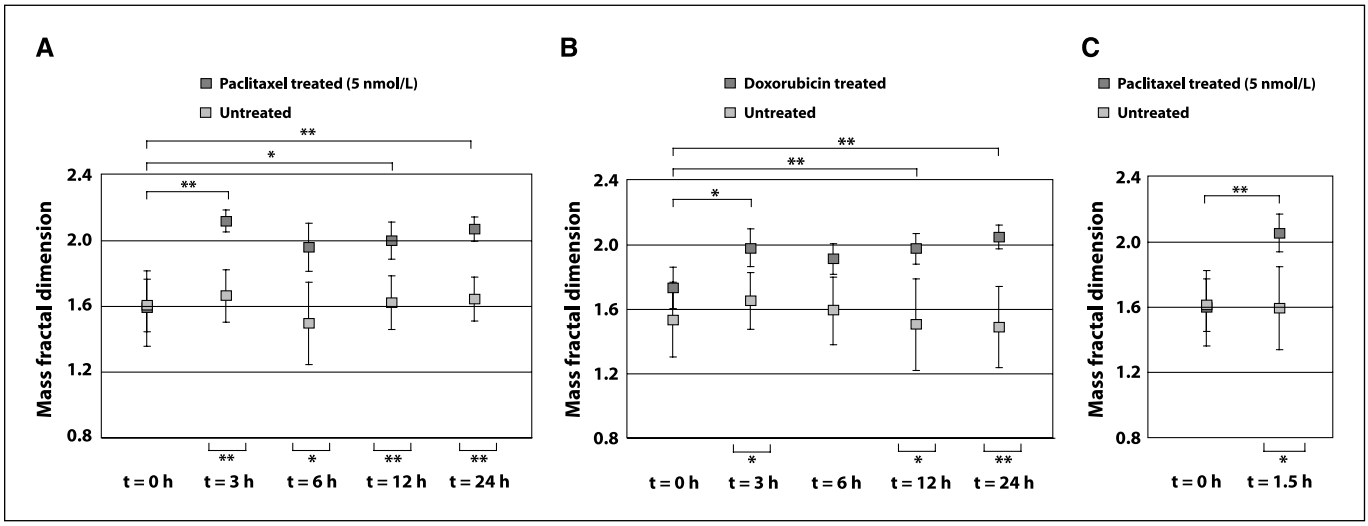

Figure 3. Paclitaxel and doxorubicin induce a significant change in the mass FD of MCF-7 cells. Summary of mass FD results for MCF-7 cells treated with (*A*) 5 nmol/L Paclitaxel and (*B*) 5 μmol/L Doxorubicin at t = 3, 6, 12, and 24 h posttreatment. *C,* comparison of cells treated with 5 nmol/L Paclitaxel and controls at t = 1.5 h. 50 nmol/L Paclitaxel treatment results are shown in Supplementary Fig. S3. *, statistical significance ($P < 0.05$); **, high statistical significance ($P < 0.001$).

were either left untreated (control) or treated with doxorubicin for 3, 6, 12, and 24 hours. In doxorubicin-treated MCF-7 cells, the mass FD increased from D = 1.76 ± 0.17 at t = 0 hours to D = 1.98 ± 0.21 at t = 3 hours and then regressed slightly to D = 1.92 ± 0.21 at t = 6 hours. The mass FD increased to 2.00 ± 0.16 at t = 12 hours and to 2.06 ± 0.09 at 24 hours. The mass FD of control cells range from 1.50 to 1.75 with SDs ranging from 0.15 to 0.40. The mass FD of treated cells at t = 3, 12, and 24 hours represents statistically significant differences from control cells and treated cells at t = 0 hours (Fig. 3*B*) with again no statistically significant differences seen between the t = 0-hour and the t = 6-hour time point.

To investigate if changes could be detected at earlier time points, MCF-7 cells were treated with 5 nmol/L paclitaxel and compared with control cells at t = 1.5 hours posttreatment. The T matrix–based ILSA algorithm determines the mass FD to be D = 2.05 ± 0.20 at this time point, compared with D = 1.59 ± 0.26 for the control cells, a statistically significant difference ($P < 0.05$). The mass FD of treated cells at t = 1.5 hours represents a highly statistically significant difference from control cells and treated cells at t = 0 hours (Fig. 3*C*).

MCF-7 cells treated with 50 nmol/L paclitaxel arrest in the G_2-M phase of the cell cycle (Fig. 1). Therefore, to determine if the a/LCI mass FD results are indicative of apoptosis, MCF-7 cells were either left control or treated with 50 nmol/L paclitaxel for 3, 6, 12, and 24 hours (Supplementary Fig. S5). Interestingly, there is a significant difference between the mass FD of treated cells and control cells at t = 3 hours, after which point the mass FD recovered to the same as control cells; no statistically significant differences exist beyond 3 hours.

QIA box counting FD of cell nuclei. The box FD was computed by QIA of images (Fig. 4*A* and *B*) taken from DAPI-stained MCF-7 cells either left untreated or treated with 5 nmol/L paclitaxel. The FD of treated cells increased from 1.62 ± 0.08 at t = 3 hours to 1.64 ± 0.05 at t = 6 hours to 1.71 ± 0.08 at t = 12 hours and t = 24 hours. The box FD of control cells was between 1.60 and 1.62 with a SD of 0.05 at all time points. The differences between FD of treated and control cells are statistically significant at t = 12 and 24 hours. See Fig. 5*A* for a summary of results.

QIA box counting FD of mitochondria. The box FD was computed by QIA of images (Fig. 4*C* and *D*) taken from MitoTracker FM Green-stained MCF-7 cells treated with 5 nmol/L paclitaxel and control samples. The box FD of treated cells at t = 3 hours was 1.65 ± 0.07, whereas the FD of control cells at t = 3 hours was 1.60 ± 0.06. The box FD of treated cells at t = 6 hours was 1.60 ± 0.08, whereas the box FD of control cells at t = 6 hours was 1.56 ± 0.08. Finally, the box FD of treated cells at

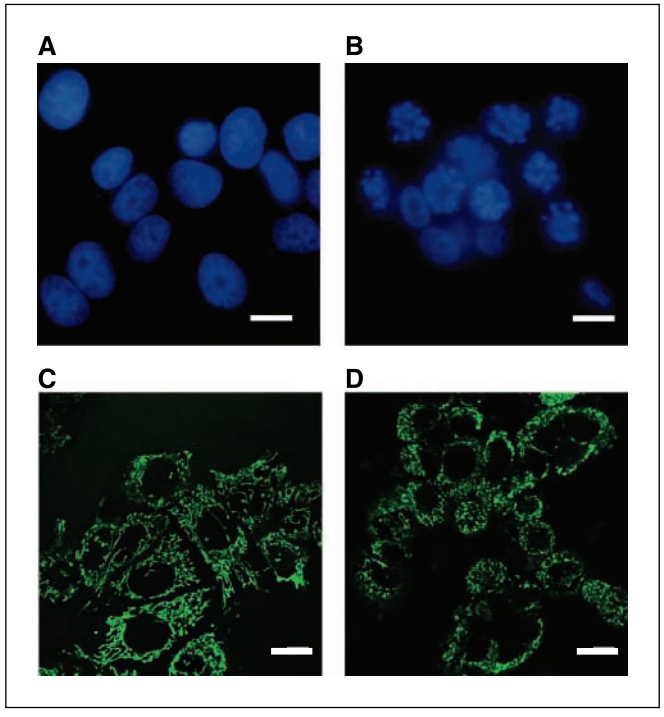

Figure 4. DAPI and MitoTracker images from paclitaxel-treated MCF-7 cells. Representative images from DAPI (*A* and *B*) and MitoTracker (*C* and *D*) stained control (*A* and *C*) and paclitaxel-treated (*B* and *D*) MCF-7 cells. *Scale bars,* 10 μm.

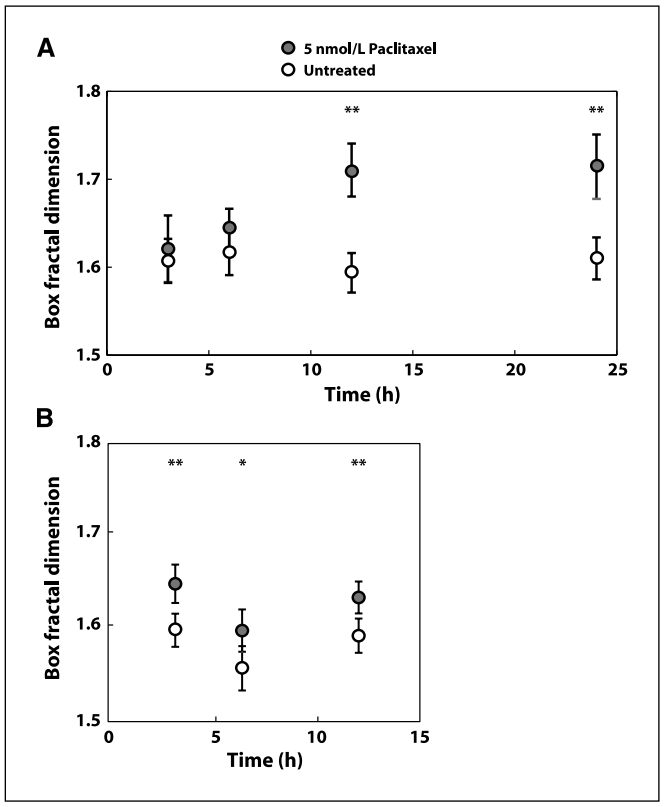

Figure 5. Paclitaxel induces a significant change in the box FD of MCF-7 cell nuclei and mitochondria. Nuclei (*A*) and mitochondria (*B*) after treatment with 5 nmol/L Paclitaxel for 3, 6, 12, and 24 h or 3, 6, and 12 h, respectively. For nuclei, box FD is assessed by QIA of DAPI-stained images using fluorescence microscopy. For mitochondria, box FD is assessed by QIA of MitoTracker FM Green-stained images using confocal fluorescence microscopy.

t = 12 hours was 1.63 ± 0.06, whereas the box FD of control cells at t = 12 h was 1.59 ± 0.07. At each time point, the difference in box FD between treated and control cells is statistically significant ($P < 0.05$), and the difference at t = 3 hours and t = 12 hours is highly significant ($P < 0.001$). See Fig. 5*B* for summary of results.

Discussion

Fractal dimension is a measure of the texture of an object: as a mass distribution transitions from a fine, smooth structure to a coarser, grainer structure, the FD increases. We have shown that the mass FD of MCF-7 cells, assessed through the angular light scattering profile, provides an early and sensitive indication of apoptosis. More specifically, in both doxorubicin- and paclitaxel-treated cells, the mass FD increases dramatically, with an increase of up to 30% soon after treatment, and remains at an elevated level as the cells undergo apoptosis. Differences for both types of treatment are statistically significant shortly after treatment (1.5–3 hours posttreatment) as well as at later time points, when the cells present more traditional markers of apoptosis induction (12 and 24 hours posttreatment). The fact that statistically significant changes in FD are seen for both treatments indicates that the changes are not drug specific.

We hypothesized that the mass FD would change as the cells underwent apoptosis due to nuclear fragmentation and/or condensation. Analysis of DAPI-stained images indicated that the box FD did increase to elevated levels at 12 and 24 hours, which could explain the elevated mass FD assessed by a/LCI at those time points. More surprising, and more significant, was the finding of early changes in mass FD, as early as 1.5 hours in 5 nmol/L paclitaxel-treated cells. It is probable that this change occurs due to structural changes in another organelle. Due to the sensitivity of light scattering to mitochondrial morphology (30, 31), we hypothesized that these organelles were largely responsible for the early, and possibly, later observed changes in mass FD. Our analysis of MitoTracker FM Green–stained cells supports this hypothesis. We see significant changes in box FD after 3 hours of treatment with 5 nmol/L of paclitaxel in the mitochondria images. We note that there is an important distinction between computing box FD using fluorescence images and mass FD using a/LCI. Namely, although microscopic imaging is subject to the diffraction limit (~400 nm), a/LCI is sensitive to changes in structure well below the diffraction limit. With this in mind, we acknowledge that there are a number of other organelles that could experience structural changes due to apoptosis-related events soon after treatment. Mass FD would be sensitive to any changes in subcellular organization, even those not necessarily detectable by image analysis, provided that the affected organelles undergo topological changes that result in changes in scattered light. However, our data supports the hypothesis that the nucleus and mitochondria are both, at least partly, responsible for the changes in FD.

Two other noteworthy results are the trends in mass FD for both doxorubicin-treated and 5 nmol/L paclitaxel-treated cells, and the differences in mass FD between 50 nmol/L and 5 nmol/L paclitaxel-treated cells. First, for both 5 nmol/L paclitaxel- and doxorubicin-treated cells, there is an increase in mass FD up to 3 hours, and then a slight reversal at 6 hours followed by a steady increase through 24 hours. Although these trends are not statistically significant, they do manifest in both treatments. The presence of these trends in both treatments lends credence to the possibility that there are at least two distinct mechanisms responsible for the changes in mass FD, which occur in two different temporal windows posttreatment. Additionally, the presence of the trend for both apoptosis-inducing treatments indicates that these two distinct mechanisms are inherent to structural changes that occur during, or leading up to, apoptosis. As previously stated, our analysis indicates that mitochondrial structural changes are partly responsible for at least the early changes in mass FD, whereas nuclear substructure changes are at least partly responsible for later changes in mass FD.

The second noteworthy finding was that 50 nmol/L paclitaxel treatment caused early changes in mass FD, which then reverted to nearly the mass FD of control cells at later time points. The differences between the mass FD of 50 nmol/L paclitaxel-treated cells and control cells are not statistically significant after 3 hours. This finding is important because the 50 nmol/L paclitaxel treatment did not result in apoptosis within the observation window. This indicates that the early changes seen in mass FD are not necessarily related to apoptosis but rather to general structural changes in cellular organelles due to events that may lead to apoptosis. For example, mitochondrial changes that occur in response to cellular stress include mitochondrial swelling, and mitochondrial fission and fusion (2, 8, 9, 32). One model of apoptosis suggests that mitochondrial fission is required for and precedes the loss of mitochondrial membrane potential during apoptosis. However, there are reports that inhibition of mitochondrial fission does not block Bax/Bak-dependent apoptosis (32). Our results lend further support to the notion that later changes in

FD are related to nuclear fragmentation and apoptosis, but early changes are caused by a different cellular event that may involve mitochondrial fission.

Previous light scattering studies have explored using FD for detecting apoptosis and dysplasia, but the present study shows stark and statistically significant differences early in treatment, and across multiple treatments. The primary advance that yielded the high degree of sensitivity showed in this study is the use of a T matrix–based ILSA model that accounts for nuclear asphericity. This is in contrast to previous techniques that relied on light scattering model, which assumed spherical cell nuclei and organelles. By removing the uncertainty that arises from incompatibility between the shape of the nucleus and the light scattering models previously used in ILSA, we find that the determination of subcellular structures is more accurate and sensitive. Future applications of light scattering can exploit this increase in sensitivity by using a T matrix–based ILSA algorithm (or another light scattering model appropriate for nuclear shapes) for assessing mass FD. As a general quantitative assessment of changes in cell structure and organization, mass FD presents a potential new avenue for assessing changes in cell function including differentiation, proliferation, apoptosis, and others.

In conclusion, noninvasive, high-throughput light scattering methods such as a/LCI, are a sensitive indicator of subcellular structure. In the present study, we have used a/LCI to measure FD of subcellular structures to distinguish between cells treated with apoptosis-inducing drugs and control cells. Moreover, the mass FD of treated and control cells presents significant differences very soon after treatment. Our studies with image analysis of fluorescently tagged organelles indicates that changes in mitochondrial morphology are partly responsible for early changes in FD, whereas changes in nuclear structure are largely responsible for later changes in FD. These findings suggest that light scattering can be a powerful noninvasive tool for monitoring apoptosis in both basic research experiments and clinical treatments.

Disclosure of Potential Conflicts of Interest

No potential conflicts of interest were disclosed.

Acknowledgments

Received 8/8/2008; revised 9/18/2008; accepted 11/20/2008.

Grant support: DoD BCRP Multidisciplinary Postdoctoral Award (BC073290; J.H. Ostrander), grants from the NIH (NCI R33-CA109907, NCI R21CA120128-01; A. Wax), and the NSF (BES 03-48204).

The costs of publication of this article were defrayed in part by the payment of page charges. This article must therefore be hereby marked *advertisement* in accordance with 18 U.S.C. Section 1734 solely to indicate this fact.

We thank Stacy Millon for assistance with confocal microscopy, Yongrui Luan for assistance in calculating FDs in ImageJ, and the Duke University Comprehensive Cancer Center Flow Cytometry Core Facility and Mike Cook for advice with cell cycle experiments.

References

1. Hanahan D, Weinberg RA. The hallmarks of cancer. Cell 2000;100:57–70.
2. Taylor RC, Cullen SP, Martin SJ. Apoptosis: controlled demolition at the cellular level. Nat Rev 2008;9:231–41.
3. Blankenberg FG. *In vivo* detection of apoptosis. J Nucl Med 2008;49 Suppl 2:81–95S.
4. Guo B, Hembruff SL, Villeneuve DJ, Kirwan AF, Parissenti AM. Potent killing of paclitaxel- and doxorubicin-resistant breast cancer cells by calphostin C accompanied by cytoplasmic vacuolization. Breast Cancer Res Treat 2003;82:125–41.
5. Saunders DE, Lawrence WD, Christensen C, Wappler NL, Ruan H, Deppe G. Paclitaxel-induced apoptosis in MCF-7 breast-cancer cells. Int J Cancer 1997;70:214–20.
6. Krysko DV, Vanden Berghe T, D'Herde K, Vandenabeele P. Apoptosis and necrosis: detection, discrimination and phagocytosis. Methods 2008;44:205–21.
7. Kaufmann SH, Lee SH, Meng XW, et al. Apoptosis-associated caspase activation assays. Methods 2008;44:262–72.
8. Cereghetti GM, Scorrano L. The many shapes of mitochondrial death. Oncogene 2006;25:4717–24.
9. Frank S, Gaume B, Bergmann-Leitner ES, et al. The role of dynamin-related protein 1, a mediator of mitochondrial fission, in apoptosis. Dev Cell 2001;1:515–25.
10. Lane JD, Lucocq J, Pryde J, et al. Caspase-mediated cleavage of the stacking protein GRASP65 is required for Golgi fragmentation during apoptosis. J Cell Biol 2002;156:495–509.
11. Brown WJ, Pyhtila JW, Terry NG, et al. Review and recent development of angle-resolved low-coherence interferometry for detection of precancerous cells in human esophageal epithelium. IEEE J Sel Top Quant Elec 2008;14:88–97.
12. Pyhtila JW, Graf RN, Wax A. Determining nuclear morphology using an improved angle-resolved low coherence interferometry system. Opt Express 2003;11:3473–84.
13. Wax A, Yang CH, Backman V, et al. Cellular organization and substructure measured using angle-resolved low-coherence interferometry. Biophys J 2002;82:2256–64.
14. Krug JT, Wang GD, Emory SR, Nie SM. Efficient Raman enhancement and intermittent light emission observed in single gold nanocrystals. J Am Chem Soc 1999;121:9208–14.
15. Wax A, Yang CH, Muller MG, et al. *In situ* detection of neoplastic transformation and chemopreventive effects in rat esophagus epithelium using angle-resolved low-coherence interferometry. Cancer Res 2003;63:3556–9.
16. Chalut KJ, Kresty LA, Pyhtila JW, et al. *In situ* assessment of intraepithelial neoplasia in hamster trachea epithelium using angle-resolved low-coherence interferometry. Cancer Epidemiol Biomarkers Prev 2007;16:223–7.
17. Chalut KJ, Chen S, Finan JD, et al. Label-free, high-throughput measurements of dynamic changes in cell nuclei using angle-resolved low coherence interferometry. Biophys J 2008;94:4948–56.
18. Levitt JM, Hunter M, Mujat C, McLaughlin-Drubin M, Munger K, Georgakoudi I. Diagnostic cellular organization features extracted from autofluorescence images. Opt Lett 2007;32:3305–7.
19. Kim YL, Liu Y, Wali RK, et al. Simultaneous measurement of angular and spectral properties of light scattering for characterization of tissue microarchitecture and its alteration in early precancer. IEEE J Sel Top Quant Elec 2003;9:243–56.
20. Wilson JD, Bigelow CE, Calkins DJ, Foster TH. Light scattering from intact cells reports oxidative-stress-induced mitochondrial swelling. Biophys J 2005;88:2929–38.
21. Mulvey CS, Curtis AL, Singh SK, Bigio IJ. Elastic scattering spectroscopy as a diagnostic tool for apoptosis in cell cultures. IEEE J Sel Top Quant Elec 2007;13:1663–70.
22. Boustany NN, Tsai YC, Pfister B, Joiner WM, Oyler GA, Thakor NV. BCL-x(L)-dependent light scattering by apoptotic cells. Biophys J 2004;87:4163–71.
23. Wilson JD, Giesselman BR, Mitra S, Foster TH. Lysosome-damage-induced scattering changes coincide with release of cytochrome c. Opt Lett 2007;32:2517–9.
24. Pyhtila JW, Simnick AJ, Chilkoti A, Wax A. Analysis of long range correlations due to coherent light scattering from in-vitro cell arrays using angle-resolved low coherence interferometry. J Biomed Opt 2006;11:034022.
25. Mishchenko MI, Travis LD, Hovenier JW. Light scattering by nonspherical particles: theory, measurements and applications. San Diego; London: Academic; 2000.
26. Amoozegar C, Giacomelli MG, Keener JD, Chalut KJ, Wax A. Experimental verification of T matrix based inverse light scattering analysis for assessing structure of spheroids as models of cell nuclei. Appl Opt. In press 2009.
27. Giacomelli M, Chalut KJ, Ostrander JH, Wax A. Application of T-matrix method to determine the structure of spheroidal cell nuclei with angle-resolved light scattering. Opt Lett 2008;33:2452–4.
28. Teixera J. Experimental methods for studying fractal aggregates. In: Stanley HE, Ostrowsky N, editors. On Growth and Form, Fractal and Non-Fractal Patterns in Physics; 1986. p. 145–62.
29. Schmitt JM, Kumar G. Turbulent nature of refractive-index variations in biological tissue. Opt Lett 1996;21:1310–2.
30. Boustany NN, Drezek R, Thakor NV. Calcium-induced alterations in mitochondrial morphology quantified *in situ* with optical scatter imaging. Biophys J 2002;83:1691–700.
31. Wilson JD, Foster TH. Mie theory interpretations of light scattering from intact cells. Opt Lett 2005;30:2442–4.
32. Parone PA, James DI, Da Cruz S, et al. Inhibiting the mitochondrial fission machinery does not prevent Bax/Bak-dependent apoptosis. Mol Cell Biol 2006;26:7397–408.